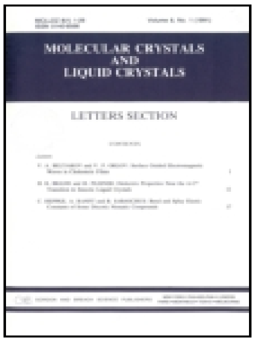

Taylor & Francis
Taylor & Francis Group

Molecular Crystals and Liquid Crystals

ISSN: 1542-1406 (Print) 1563-5287 (Online) Journal homepage: http://www.tandfonline.com/loi/gmcl20

Growth of Diamond-Like Carbon and Icosahedral Boron Carbide by Chemical Vapor Deposition System

M. Ghoranneviss & A. Salar Elahi

To cite this article: M. Ghoranneviss & A. Salar Elahi (2015) Growth of Diamond-Like Carbon and Icosahedral Boron Carbide by Chemical Vapor Deposition System, Molecular Crystals and Liquid Crystals, 608:1, 223-236, DOI: 10.1080/15421406.2014.967745

To link to this article: http://dx.doi.org/10.1080/15421406.2014.967745

Mol. Cryst. Liq. Cryst., Vol. 608: pp. 223–236, 2015

ISSN: 1542-1406 print/1563-5287 online
DOI: 10.1080/15421406.2014.967745

Growth of Diamond-Like Carbon and Icosahedral Boron Carbide by Chemical Vapor Deposition System

M. GHORANNEVISS AND A. SALAR ELAHI*

Plasma Physics Research Center, Science and Research Branch, Islamic Azad University, Tehran, Iran

Diamond-like carbon (DLC) possesses an array of valuable properties: outstanding abrasion and wear resistance; chemical inertness; exceptional hardness; low coefficient of friction; and high dielectric strength. Methods used to deposit DLC include ion beam deposition, cathodic arc spray, pulsed laser ablation, argon ion sputtering, and plasma-enhanced chemical vapor deposition. In the present work, carbon nano-structures were doped by boron atoms to synthesize icosahedral boron carbide using Hot Filament Chemical Vapor Deposition (HFCVD) *system. Raman spectroscopy, X-ray diffraction technique, Debye-Scherrer calculation, Tuinstra-Koenig formula and scanning electron microscopy results were presented and discussed.*

Keywords Boron carbide; CVD; DLC

1. Introduction

Chemical Vapor Deposition (CVD) is a technique used to produce solid materials, typically thin films. In CVD processes, substrates are heated to high temperatures and exposed to precursor materials in the gaseous state. The precursors react or decompose on the substrate surface to yield a coating of the required material. To a large extent, process success depends on system conditions. CVD schemes are employed widely for various processes throughout the semiconductor industry. Although CVD was not involved in the initial discoveries of graphene and carbon nano-tubes (CNTs), it has been found subsequently to be an excellent, scalable method for the production of high-quality material. Hot Filament CVD (HFCVD) is a major method of diamond and diamond-like carbon (DLC) deposition. Most advantages of HFCVD are: it has high resolution, HFCVD apparatus is much simpler, and it is much easier to enlarge the deposition area in HFCVD at a much lower cost. DLC is an amorphous carbon material made of random networks of sp^3 and sp^2 hybrid bonds. DLC material with high sp^3 content has similar properties as single crystal or polycrystalline diamond. They are hard, electrically insulating, chemically inert, very good heat conductors, that they show high electron and hole mobility, negative electron affinity, high breakdown field, light weight, large band gaps ($>> 2$ eV), and a high index of refraction

*Address correspondence to A. Salar Elahi, Plasma Physics Research Center, Science and Research Branch, Islamic Azad University, Tehran, Iran. Email: Salari_phy@yahoo.com

Color versions of one or more of the figures in the article can be found online at www.tandfonline.com/gmcl.

($n >> 2$). Owing to these properties, DLCs are extensively used in diverse fields, such as wear coatings, microelectronics, micro-tribology, and biomedical technology. However their insulating properties and wide band gap lead to limitation of their applications in electronics (Unless the charge carriers incorporated into them [1–5]). Furthermore, by various boron to carbon stoichiometry, the ratio higher than 2, are known as boron carbides. Boron carbide exists as a stable single phase compound in a large homogeneity range from 8%up to 20% C concentrations [6]. Boron atom suppresses the formation of sp^2 graphitic clusters and increases both the sp^3 bonding and the hydrogen content in the DLC films [7]. Consequently, the electrical conductivity of the film is a complicated function of the combined effects of the boron-doping level, the grain boundaries, and the impurities. As the grain size in the films becomes smaller, i.e. from Microcrystalline Diamond (MCD) to Nanocrystalline Diamond (NCD), the relative importance of these grain boundaries increases [8, 9]. $B_{13}C_2$ is an attractive hard coating for a variety of applications interestingly [9]. Its high melting point, high modulus, large neutron capture section, low density, chemical inertness, outstanding thermal and electrical properties make boron carbide a strong candidate for high technology applications [10–14]. Recently boron-doped diamond or DLC films have been prepared by an assortment of methods including: microwave plasma CVD, plasma-enhanced CVD, photochemical vapor deposition (photo-CVD), DC saddle-field glow-discharge deposition, Pulsed Laser Deposition (PLD) and plasma immersion ion processing [15]. The aim of this research is to present experimental results on the synthesis of DLC and $B_{13}C_2$, nanostructure, chemical composition, deposition rate using HFCVD and to discuss the influence of boron content on the surface morphology, crystallographic structure of the deposited films.

2. Experimental Details

B-doped DLC films were synthesized with an HFCVD method. The DLC films with different boron-doping levels were produced using solutions with varying boron (B) concentrations, i.e., 0.00626, 0.0125, 0.025 and 0.05 molars (or 0.37×10^1, 7.5×10^{13}, 150×10^{13} and 3011×10^{13} ppm). The growth process was triggered upon introducing hydrogen gas (H_2) passing through ethanol as B_2O_3 solution in various concentrations in ethanol, as well as boron and carbon source into the chamber. A pure hydrogen gas flow rate of approximately 100 sccm regulated by precision mass flow meter and a total pressure of 15 Torr were maintained throughout the experiment as shown schematically in Fig. 1. The substrate temperature was 500°C measured by a thermocouple mounted on the substrate surface. Initially, a P-type silicon wafer (100) was cut in 1×1 cm^2 pieces and then ultrasonically cleaned in acetone, ethanol and deionized water, respectively, each for 10 minutes. Subsequently, Fe films for has been high surface reactivity and absorptivity were sputtered by DC-Magnetron Sputtering with 13 nm thickness measured by Rutherford Back Scattering (RBS) technique as shown in Fig. 2. Substrates were then placed on the sample platform with a distance of 1 cm between Si substrate and the hot-filament. Prior to synthesis, etching was performed in H_2 ambient for 10 minutes. Figure 3 illustrates surface roughness before and after etching 0.8 and 26.20 nm respectively.

The deposition duration of all samples was kept at 30 min in this research. For investigating the surface morphology of the as-grown boron-doped DLC films, a field emission scanning electron microscope (FE-SEM) 15 KV was used. Further, the crystallinity and quality of the synthesized structures were characterized by a fully automatic X-ray diffractometer ($\lambda = 1.54$ nm, D/Max = 2200) using a Philips diffractometer with CuKα1

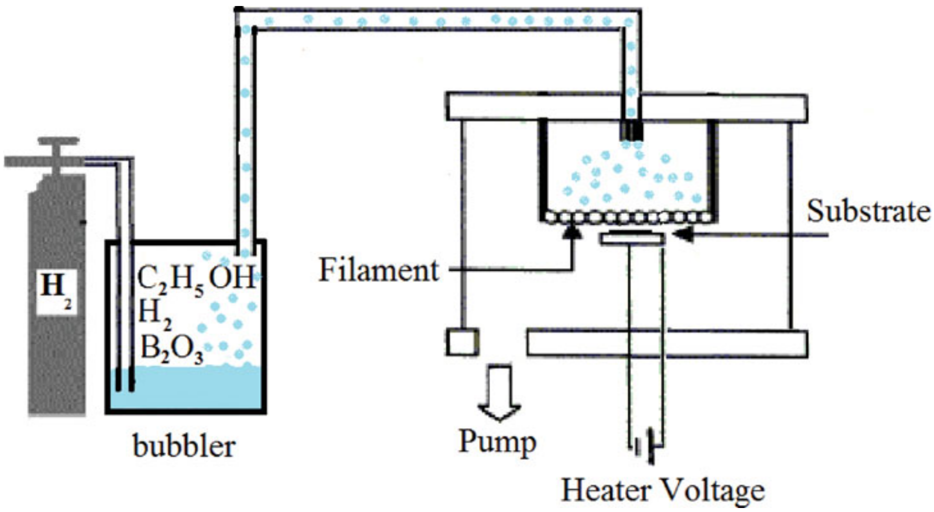

Figure 1. Schematic of HFCVD used in experiment.

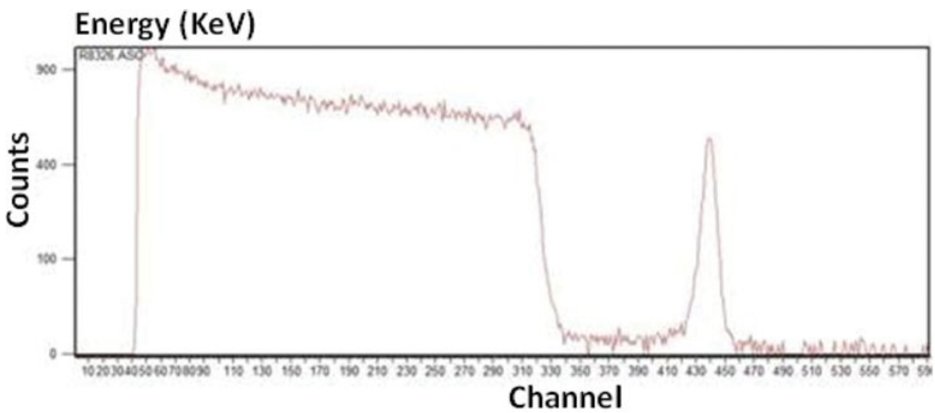

Figure 2. Rutherford back scattering (RBS) show thickness Fe layer deposited on silicon 13 nm.

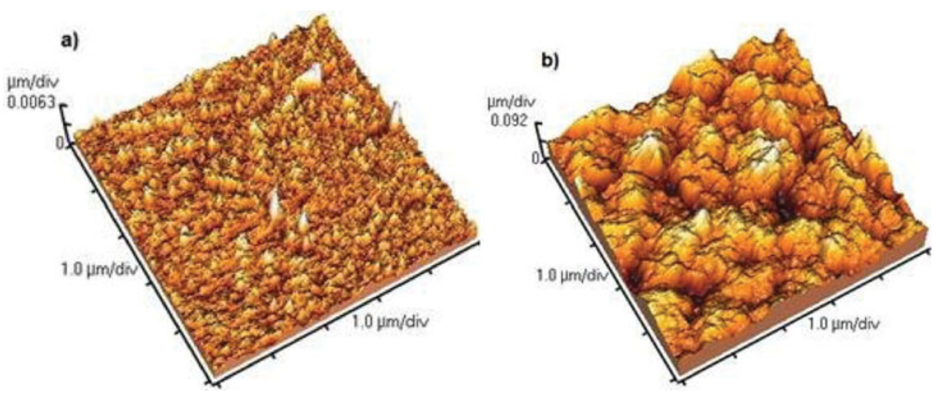

Figure 3. The AFM image of the silicon substrate coated with Fe (a) before etching and (b) after etching by H_2 gas.

radiation with an incident angle of 5°. Moreover, Raman spectroscopy was utilized to study the composition of structure. Transmission Electron Microscopy (TEM) images disclosed constrictions clusters in structure.

3. Results and Discussion

Figure 4 shows the XRD patterns of the B-doped DLC films. All XRD peaks at 23.60°, 40.32°, 48.25°, 53.40°, 75.43°, 80.55° originated from $B_{13}C_2$ relevant to standard card and the peak at 69.17° arose from the silicon substrate. According to XRD results, the average crystal size of nanocrystals was between 5–80 nm that has been calculated by Debye-Scherr formula.

$$D = 0.9 \times \lambda/(\beta Cos\theta_\beta), \tag{1}$$

where D = thickness of crystallite, K = constant dependent on crystallite shape 0.9, λ = X-ray wavelength, β = FWHM, and Θ_β = Bragg angle. An effect of the finite crystallite sizes is seen as a broadening of the peaks in an X-ray diffraction as is explained by the Equation (1). The XRD patterns of the $B_{13}C_2$ icosahedral boron Carbide film is dominated by the peaks at 23.60°, 48.25°, and 53.40° corresponding to planes (0 1 2), (0 2 4), and (2 0 5) of boron carbide icosahedral, diffraction peaks evidence the presence of crystalline $B_{13}C_2$. FWHM had been similar treatment see Fig. 5.

$$\text{By using}\ \delta = 1/D^2, \tag{2}$$

where δ = liner dislocation, D = thickness of crystallite and Stokes and Wilson formula

$$\varepsilon = \beta/4\tan\Theta\beta, \tag{3}$$

Θ_β = Bragg angle, β = FWHM, see Table 1 by increasing level doping decreased dislocations in layers and tension also layers was better constructed. Also, numbers of crystals per unit area:

$$N = t/D^3, \tag{4}$$

where t = thickness film, D = thickness of crystallite boron carbide icosahedral.

4. The Raman Spectrum of Boron-Doped DLC

Raman spectroscopy is a spectroscopic technique based on inelastic scattering of monochromatic light, usually from a laser source. Inelastic scattering means that the frequency of photons in monochromatic light changes upon interaction with a sample. Photons of the laser light are absorbed by the sample and then reemitted. Frequency of the reemitted photons is shifted up or down in comparison with original monochromatic frequency, which is called the Raman effect. This shift provides information about vibrational, rotational and other low frequency transitions in molecules. Raman spectroscopy can be used to study solid, liquid and gaseous samples. Raman spectroscopy is regarded as a widespread, nondestructive technique for characterizing various carbon structures [16] and has been extensively used for B13C2 characterization [17,18]. Being able to discriminate between sp2 and sp3 carbon sites, it is the most commonplace method utilized for corroborating the quality of crystalline films. Therefore, by using Raman spectroscopy, it is straightforward

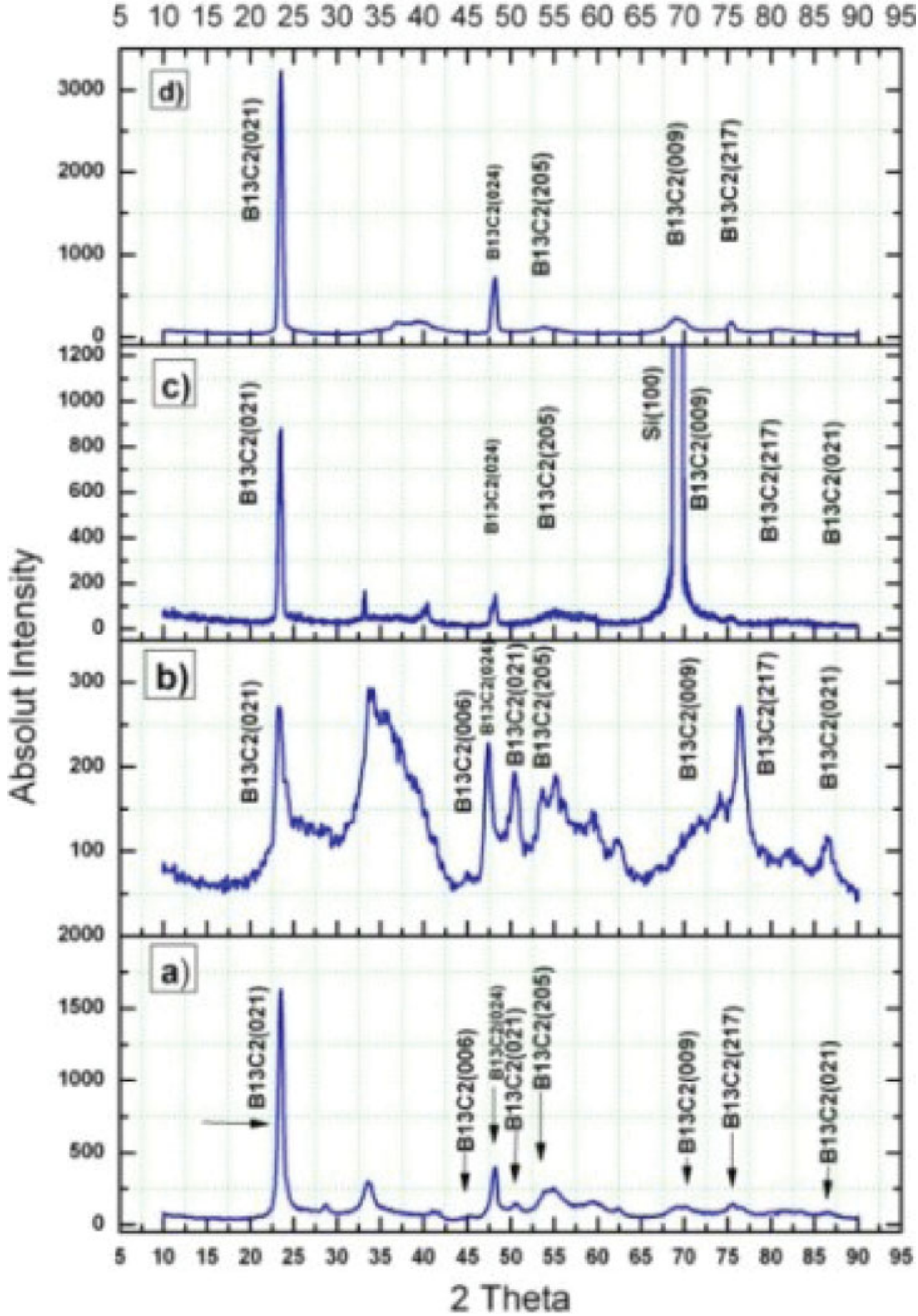

Figure 4. XRD patterns of B-doped DLC films with different contents of boron: 0.00625, 0.0125, 0.025 and 0.05 molar from a-d, respectively. In c) profile was removed silicon (100) peak.

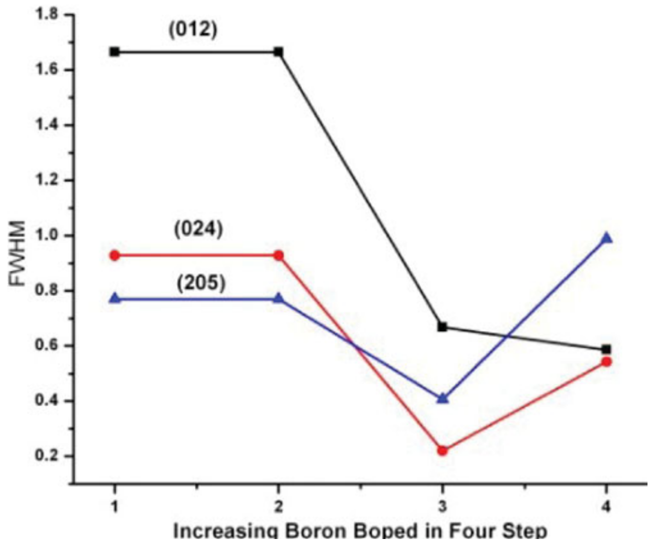

Figure 5. FWHM of peaks (012), (024), (205) in icosahedral boron carbide.

to distinguish involvements of B13C2 from the modes of the aromatic sp2 clusters observed at higher frequencies. However, the roots of some B13C2 peaks are still debatable. One of the B13C2 modes is found around 275 cm-1–325 cm-1. The other B13C2 modes at 650–1000 cm^{-1} also put the same scaling characteristic on view. In addition to information about the boron carbide phase, substantial insight into the presence of free carbon in B13C2 can also be obtained by careful Raman analysis [17]. By adroitly analyzing Raman results, one is able to attain significant knowledge concerning the existence of free carbon in B13C2 as well as figuring out the boron Carbide phase. The first-order Raman spectrum of graphitic single crystals is only peaked at 1589 cm^{-1} (G-peak), which is the fingerprint of stretching vibrations of double, C = C, bonds. In the presence of graphitic domains of finite size, amorphization of the graphene layer, or defects, a second peak emerges at 1300 cm^{-1}–1360 cm^{-1} (D-peak) which can be assigned to breathing vibrations of aromatic 6-fold rings in finite graphitic domains. At visible or near infrared excitation wavelength, λ, the diameter, L, of the sp^2 domain has peculiarly shown to affect the ID/IG ratio [17, 18]. The whole selection rules can be disregarded while at a higher degree of disorder, and the total density of phonons can be observed. Particularly, at 1350 cm^{-1} and 1580 cm^{-1}, phonons can be observed illustrating the existence of microcrystalline graphite and the scattering intensity in the 1400–1600 cm^{-1} region will be due to non-diamond-carbon impurities [19, 20]. Raman spectroscopy is a popular, non-destructive tool for structural characterization of carbons. It is traditionally carried out at the commonly available wavelengths in the blue–green spectral region (488–514.5 nm), but multi wavelength Raman studies are becoming increasingly used. Recently there has been a considerable improvement in the field of Raman spectroscopy in carbon systems. In particular, the appreciation of the strict correlation of the Raman process with the electronic properties of carbon systems is a major driving force to further develop all the possibilities of this versatile technique. As indicated in Fig. 6, peaks at 280 cm^{-1}, 750 cm^{-1}, 1340 cm^{-1}, and 1580 cm^{-1} were detected in Raman spectra. The peaks appeared at 280 cm^{-1} and 750 cm^{-1} are associated with boron carbide icosahedral. Despite the frequent appearance of Raman peaks in the 250 cm^{-1} to 350 cm^{-1}

Table 1. Peak with highest intensity signifying

Sample	FWHM (0 1 2)	Crystal size (nm)	FWHM (0 2 4)	Crystal size (nm)	FWHM (2 0 5)	Crystal size (nm)	c/a	$N.10^{19}$ (L^{-2})	$\delta.10^{15}$ (Line/m^2)	$\varepsilon.10^{-3}$ (Lin^{-2}/m-^{2})
(a)	0.7147	1.89	0.7436	2.04	0.8498	1.82	1.044465962	1.728024042	8.26446281	2.99332617
(b)	1.6642	0.85	0.9277	1.63	0.7702	2.01	1.044465983	35.9	40	5.754393988
(c)	0.6676	2.12	0.2202	6.89	0.4066	3.81	2.335496874	1.331088519	6.944444444	2.7933653593
(d)	0.5861	3.48	0.5427	2.79	0.9885	1.40	2.335492276	0.8381924198	5.102040816	2,538628893

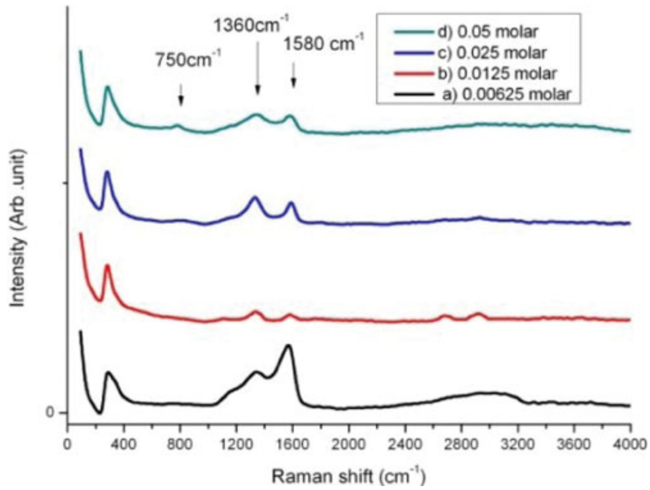

Figure 6. Raman spectra from samples shows evolutions in positions, intensity and FWHM of peaks from a) 0.00625 b) 0.0125 c) 0.025 and d) 0.05 molar boron doped in DLC films.

region in $B_{13}C_2$ ceramics, a good knowledge of their origin has not yet been acquired [21–23]. The peak at $\sim$750 cm^{-1} is related to icosahedral mode which is not sensitive to annealing, in agreement with infrared spectroscopy results. No sign of graphitic inclusions was observed [24]. The peaks centered at 1349 and 1580 cm^{-1}, are known as D and G bands, respectively. Owing to the restricted dimensions of the crystallites, a slight breaking of the selection rules may occur and the phonons located adjacent to the center of Brillouin zone scatter the incident photons. At a greater level of disorder, all of the selection rules can be 11 broken, and the total density of phonons can be observed. The G peak exhibits region

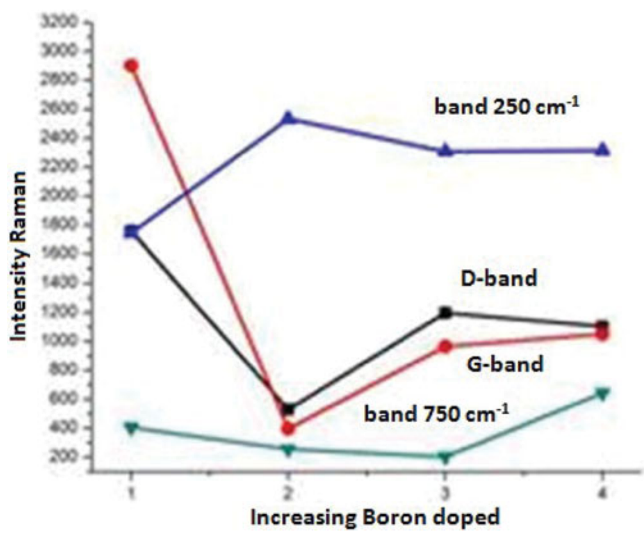

Figure 7. profile of variation in Intensity four bands 280 cm^{-1},750 cm^{-1}, D band and G band at Raman spectrum by increasing boron doped.

Table 2. Summarize data Raman

Sample	280 bond (cm^{-1})	Intensity	FWHM (cm^{-1})	750 bond (cm^{-1})	Intensity	FWHM (cm^{-1})	D-bond (cm^{-1})	Intensity	FWHM (cm^{-1})	G-bond (cm^{-1})	Intensity	FWHM (cm^{-1})	I_D/I_G	La (nm)
(a)	314	1744	88.44	775	395	97.5	1361.5	1758	370	1539	2901	170	0.60	73
(b)	287.5	2533	48	777	265	215	1333.6	530	94	1584	400	81	1.32	58.3
(c)	286.7	2300	52.5	775	184	1856	1328	1197	118	1581	965	89.6	1.24	35.48
(d)	298.6	2315	79	779	640	128	1339.9	1103	255	1551.8	1051	322	1.04	41.94

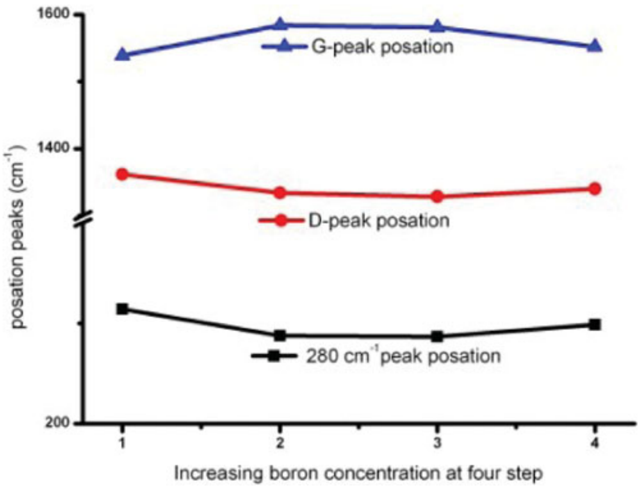

Figure 8. profile of variation in position peaks at raman spectrum by increasing boron doped.

center phonons of E_{2g} symmetry and D peak reveals K-point phonons of A_{1g} symmetry of graphite [25, 26]. Sharp G and D peaks observed around 1573 cm^{-1} and 1340 cm^{-1} suggest the presence of some species such as monocrystalline graphite in the films. The formation of sp^2 hybridized aromatic C rings and localized amorphization in $B_{13}C_2$ can be evidently deduced from the development of these peaks for all types of samples. Further, a higher level of structural damage or amorphization in $B_{13}C_2$ is concluded when more intense G and D peaks are obtained by doping boron [27–32]. Moreover, Fig. 7 shows that by increasing content B-alloyed DLC film has an intensity decrease of G-band and D-band and 750 cm^{-1} band and then increase the intensity. The broadening of the G-band relies on the increase of mass density and hardness of DLC films that it had result of added boron to films. The size of the graphite crystallites is inversely proportional to the I_D/I_G ratio, in other words, $I_D/I_G = C/L_a$, where L_a is the sp^2 correlation length or in-plane crystallite size. The broadening of G-band along with the simultaneous decrease of I_D/I_G, accompanied by the coexistent downshift in both G and D peaks, as shown in Table 2, could lead us to the conclusion that incorporating B into DLC films facilitates the formation of a film with a boosted sp^3 bonding structure. Moreover, the decrease observed in the intensity of G and D peaks stem from disrupting the vibrational behavior of the film and diminution of polarizability in the molecules of the lattice. The decrease of polarizability the promotion of a great fraction of δ bonds between B and C atoms [33, 34, 15]. In Table 2 G-peak FWHM, (I_D/I_G) and in Fig. 8 the G and D peak positions, as a function of the chemical composition of the films are illustrated. By comparing the data measured from the DLC films [7, 15, 20] with those from B-DLC films, it can be seen that incorporation of B into DLC films brings on the concurrent transfer of both G and D peak positions towards lower Raman frequencies which signifies the evolution of sp^3 fourfold coordinate bonding in the amorphous carbon films. According to Fig. 8, the dispersion in G-band towards higher wavelengths due to the grain size reduction from 73 nm to 42 nm and the subsequent phonon confinement which induces phonons away from Γ to be involved with $q = 1/L_a$. According to Tuinstra-Koening formula (Eq. (5)), L_a decreases with the increase of the intensity of appears as a result of defects in the structure [35] that surely it was result of doped boron. Tuinstra–Koening

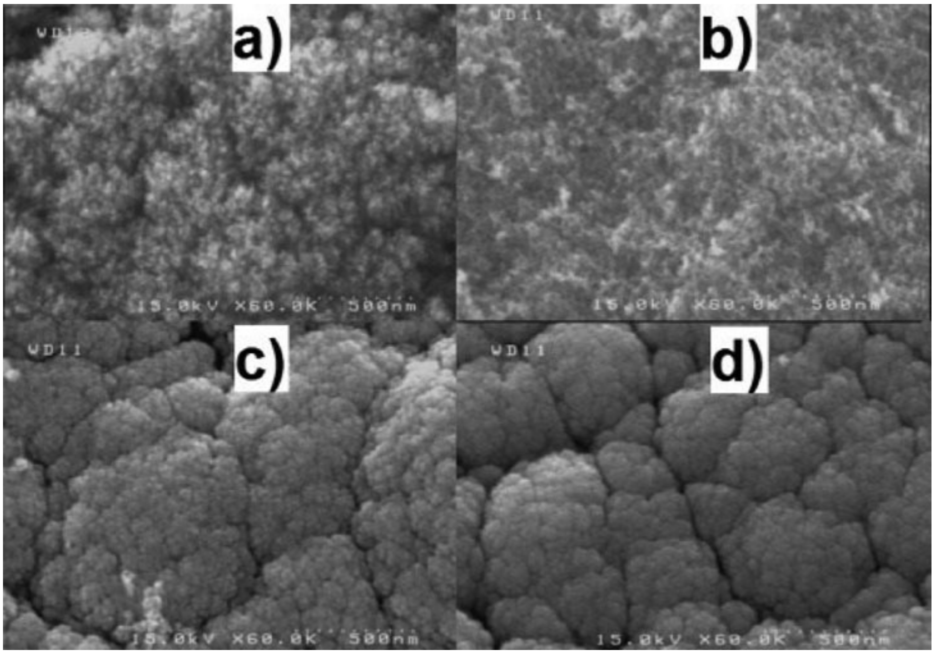

Figure 9. FE-SEM images show boron doped DLC films in different contents a) 0.00625, b) 0.0125, c) 0.025 and d) 0.05 molar. visible by Increase of cracks on surface of the structure in Fig. 6(a),(c) and (d) are relatively to doped boron in the grown film.

formula is:

$$I_G/I_D = c/La \tag{5}$$

Figure 9 shows the FE-SEM images of B-doped DLC films. The FE-SEM results indicate that the cracks exist all over the surface and relatively increase by raising the amount of dopant. In Fig. 9(a) it can be seen that, there are low cracks and shallow and the crack paths are not straight on the surface. On the other hand, Fig. 9(a) and (d), show that the surface of the coated film has particle-like features with less than 1 micrometer in diameter. Small, non-regularly shaped surface voids are also detected. For samples in Fig. 9(d), the congeries is very different from that in Fig 9(a). In Fig. 9(d), the multiplicity of cracks on the film surface is noticeable compared to those observed in Fig. 9(a). On the other hand, the specimen microstructure in Fig 9(b) differs very much from that of the other specimens. Increase of cracks on surface of the structure in Fig. 9(a), (c), and (d) was grown by doped boron in the film. Measurements indicate that the size of agglomerations on the surface for sample (a) is less than 1 μm and for samples (c) and (d) is less than 0.5 μm. These agglomeration phenomena on the structure surface due to the increase of doping dosage which then leads to the upsurge of cracks. It may be inferred according to the depth of cracks that agglomeration triggers from the moment growth initiates and gradually escalates as the growth time goes up and brings about more cracks on the surface. Also, in the Fig. 10, TEM image show boron doped DLC films in contents (a) 0.00625 molar, Samples were prepared by dispersing the powder products in n-hexane by ultrasonic treatment, dropping the mixture onto a porous carbon film supported on a copper grid and then drying the film in air. With the aid of Microstructure Measurement software, TEM images see Fig. 10

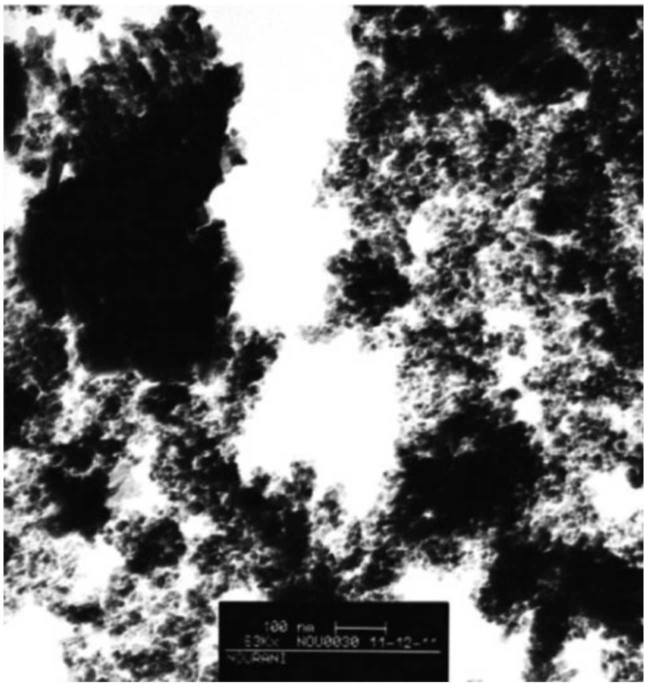

Figure 10. TEM image show boron doped DLC films in contents a) 0.00625 molar, Samples were prepared by dispersing the powder products in n-hexane by ultrasonic treatment, dropping the mixture onto a porous carbon film supported on a copper grid and then drying the film in air. With the aid of Microstructure Measurement software, TEM images see Fig. 10 illustrate that the size of produced clusters is average 22 nm.

illustrate that the size of produced clusters is average 22 nm. The spacing's were measured over different regions in the micrograph and then averaged, and results for three sample are congeries size was below 1 μm for (a) below 0.5 μm for (c) and (d) samples [36].

5. Conclusion

Hot Filament CVD (HFCVD) is a major method of diamond and diamond-like carbon (DLC) deposition. Most advantages of HFCVD are: it has high resolution, HFCVD apparatus is much simpler, and it is much easier to enlarge the deposition area in HFCVD at a much lower cost. According to XRD patterns, SEM images and raman spectra, the structure of the film was determined as DLC along with grown boron carbide icosahedrals ($B_{13}C_2$) in its texture. The size of these icosahedrals calculated by Debye–Scherrer's equation was between 5 and 80 nm. Further, the grain size has been estimated between 42 and 73 nm on the basis of raman peaks using Tuinstra-Koenig formula. Raman spectroscopy demonstrates variations in D and G peaks which are attributable to the presence of localized amorphization in $B_{13}C_2$. Additionally, the shift in G peak location towards higher wavelengths stems from the fact that owing to the diminution of grain size, phonon confinement provokes phonons to be away from Γ and contribute with $q = 1/L_a$. Also, L_a factor reduces with increasing doping amount from 73 to 42 nm. The high intensity of G-band and the low intensity of D-band in Raman spectrum in Fig. (6) black line exhibit the high degree of graphitization in matrix which increases to $I_D/I_G = 1.3$ upon raising the amount of boron incorporation in the matrix and the formation of sp^3 hybrid in the film. With further increasing the amount of boron alloy, a balance will be set between sp^2 and sp^3 hybrids in the film and the I_D/I_G ratio decreases to 1. This occurs as a result of the substitution of boron atoms with carbon atoms and the development of B-C bond. Moreover, the decrease observed in the intensity of G and D peaks stem from disrupting the vibrational behavior of the film and diminution of polarizability in the molecules of the lattice. One of the factors inducing the decrease of polarizability is the promotion of a great fraction of δ bonds between B−C atoms. The entire sp^2 sites lead to the formation of G peak. However, D peak attributes to six-fold rings. Hence, the decrease of number of rings per cluster and the increase of the fraction of chain groups gives rise to the reduction of I_D/I_G ratio. Surface morphology in SEM results discloses the growth of cauliflower structures. It is deduced that the increase of doping amount leads to creation of deep cracks on the surface and incites the reduction of the dimensions of agglomerations. Moreover, it causes damages to its uniformity which decreases with increasing doping boron from 0.5 μm to 1 μm.

References

[1] Ma, Z. Q., & Liu, B. X. (2001). Boron-doped diamond-like amorphous carbon as photovoltaic lms in solar cell. *Sol. Energy Mater. Sol. Cells*, *69*, 339–347.
[2] Nekkanty, S., & Walter, M. E. (2004). Indentation damage to boron carbide–DLC coatings with different compositions. *Surf. Coat. Technol.*, *183*, 1–9.
[3] Ullah, M., & Ahmed, E. (2012). Influence of boron carbide on properties of CVD-diamond thin films at various deposition pressures. *Curr. Appl. Phys.*, *12*, 945–957.
[4] Wang, F. M., Chen, M. W., & Lai, Q. B. (2010). Metallic contacts to nitrogen and boron doped diamond-like carbon films. *Thin Solid Films*, *518*, 3332–3336.
[5] Kautek, W., Pentzine, S., Conradi, A., Kruger, J., & Brzeinka, K.-W. (1996). Pulsed–laser deposition and boron- blending of diamond- like carbon (DLC) thin films. *Appl. Surf. Sci.*, *106*, 158–165.
[6] Conde1a, O., Silvestre, A. J., & Oliveira, J. C. (2000). Influence of carbon content on the crystallographic structure of boron carbide films. *Surf. Coat. Technol.*, *125*, 1411–1420.
[7] He, Xiao-Ming, Walter, K. C., & Nastasi, M. (2000). *J. Phys.: Condens. Matter* 12 L183 doi:10.1088/0953-8984/12/8/105
[8] May, P. W., Ludlow, W. J., Hannaway, M., Heard, P. J., Smith, J. A., & Rosser, K. N. (2008). Raman and conductivity studies of boron-doped microcrystalline diamond, facetted nanocrystalline diamond and cauliflower diamond films. *Diamond Relat. Mater.*, *17*, 105–117.
[9] Monteiro, O. R., Delplancke-Ogletree, M.-P., & Klepper, C. C. (2003). Boron carbide coatings prepared by cathodic arc deposition. *J. Mater. Sci.*, *38*, 3117–3120.
[10] Lee, K.-W., & Harris, S. J. (1998). Boron carbide films grown from microwave plasma chemical vapor Deposition. *Diamond Relat. Mater.*, *7*, 1539–1543.
[11] Sezer, A. O., & Brand, J. I. (2001). Chemical vapor deposition of boron carbide. *Mater. Sci. Eng.*, *B79*, 191–202.
[12] Lin, C.-M., Tsai, H.-L., & Yang, C. (2012). Effects of microstructure and properties on parameter optimization of boron carbide, coatings prepared using a vacuum plasma-spraying process. *Surf. Coat. Technol.*, *206*, 2673–2681.
[13] Abou Gharam, A., Lukitsch, M. J., Balogh, M. P., & Alpas, A. T. (2010). High temperature tribological behaviour of carbon based (B4C and DLC) coatings in sliding contact with aluminum. *Thin Solid Films*, *519*, 1611–1617.
[14] Eckardt, T., Bewilogua, U. K., van der Kolk, G., Hurkmans, T., Trinh, T., & Fleischer, W. (2000). Improving tribological properties of sputtered boron carbide coatings by process modifications. *Surf. Coat Technol.*, *126*, 6975–6983.

[15] Pu, J.-C., Wang, S.-F., Lin, C.-L., & Sung, J. C. (2010). Characterization of boron-doped diamond-like carbon prepared by radio frequency sputtering. *Thin Solid Films*, *519*, 521–526.
[16] Ferrari, A. C., & Robertson, J. (2004). Raman spectroscopy of amorphous nanostructure diamond like carbon and nanodiamond. *R. Soc.*, *10*, 1098–1110.
[17] Fanchini, G., & McCauley, J. W., & Chhowalla, M. (2006). Behavior of disordered boron carbideunder stress. *Phys. Rev. Lett.*, *97*, 035502–07.
[18] Vast, N., Lazzari, R., Besson, J. M., Baroni, S., & Dal Corso, A. (2000). Atomic structure and vibrational properties of icosahedral α-boron and B4C boron carbide. *Comput. Mater. Sci.*, *17*, 127–138.
[19] Kostic, R., Miric, M., Radic, T., Radovic, M., Gajic, R., & Popovic, Z. V. (2009). Optical characterization of graphene and highly oriented pyrolytic graphite. *Acta Phys. Pol. A 4*, 116–125.
[20] Ferrari, A. C. (2007). Raman spectroscopy of graphene and graphite: Disorder, electron–phonon coupling, doping and nonadiabatic effects. *Solid State Commun.*, *143*, 47–57.
[21] Ghosh, D., Subhasha, G., Lee, C. H., & Yap, Y. K. (2007). Strain-induced formation of carbon and boron clusters in boron carbide during dynamic indentation. *Appl. Phys. Lett.*, *91*, 061910–18.
[22] Hosoi, S., Kim, H., Nagata, T., Kirihara, K., Soga, K., Kimura, K., Kato, K., & Takata, M. (2007). Electron density distributions in derivative crystals of a-rhombohedral boron. *J. Phys.Soc. Jpn.*, *76*, 044602–13.
[23] H Werheit, H., Filipov, V., Schwarz, U., Armbruster, M., Leithe-Jasper, A., Tanaka, T., & Shalamberidze, S. O. 2010. *J. Phys.: Condens. Matter 22*, 045401–09, doi:10.1088/0953-8984/22/4/045401
[24] Jacobsohn, L. G., Averitt, R. D., Wetteland, C. J., Schulze, R. K., Nastasi, M., Daemen, L. L., Jenei, Z., Asoka-Kumar, P. (January 12, 2004), Experimental evidence of the role of intericosahedral chains in the hardness of boron carbide films deposited by sputtering. *Appl. Phys. Lett.*, UCRL-JRNL-201802 January 12, 2004.
[25] Baroni, N. V. S., Zerah, G., Besson, J. M., Polian, A., Grimsditch, M., & Chervin, J. C. (1997). Lattice dynamics of icosahedral α-boron under pressure. *Phys. Rev. Lett.*, *78*, 693–702.
[26] Lazzari, R., Vast, N., Besson, J. M., Baroni, S., & Corso, A. D. (1999). Structural and vibrational properties of icosahedral B4C boron carbide. *Phys. Rev. Lett.*, *83*, 3230.
[27] Tuinstra, F., & Koenig, J. L. (1970). *J. Chem. Phys.*, *53*, 1126.
[28] Al-Jishi, R., & Dresselhaus, G. (1982). *Phys. Rev. B*, *26*, 4514–4522.
[29] Ager, J., W. III., Walukiewicz, W., McCluskey, M., Plano, M. A., & Landstrass, M. I. (1995). Fano interference of the Raman phonon in heavily boron-doped diamond films grown by hemical vapor deposition. *Appl. Phys. Lett.*, *66*(5).
[30] Parthasarathy, G., Sreedhar, B., & Chetty, T. R. K. (10 April 2006). Spectroscopic and X-ray diffraction studies on fluid deposited rhombohedral graphite from the Eastern Ghats Mobile Belt, India. *Curr. Sci.*, Vol. *90*, No. 7, 10 APRIL 2006.
[31] Azevedo, A. F., Baldan, M. R., & Ferreira, N. G. (2012). Nanodiamond films for applications in electrochemical systems, hindawi publishing corporation. *Int. J. Electrochem.* Volume *2012*, Article ID 508453, 16 pages.
[32] Watanabe, T. et al (2010). Giant electric double-layer capacitance of heavily boron-doped diamond electrode. *Diamond Relat Mater*, *19*(7–9), 772–777.
[33] He, X.-M., Hakovirta, M., & Nastasi, M. (2004). Structure and properties of fluorine and boron co-alloyed diamond-like carbon films. *J. Phys. Condens. Matter.*, *16*, 8713–8724.
[34] Wu, Y.-H., Hsu, C.-M., Chia, C.-T., Lin, I.-N., & Cheng, C.-L. (2002). Field emission and Raman spectroscopy studies of atomic hydrogen etching on boron and nitrogen doped DLC films. *Diamond Relat Mater.*, *11*, 804–808.
[35] Robertson, J. (2002). diamond- like amorphous carbon. *Mater. Sci. Eng.*, *37*, 129–281.